

# Binarized 3D Whole-body Human Mesh Recovery

Zhiteng Li<sup>1</sup>, Yulun Zhang<sup>2\*</sup>, Jing Lin<sup>3</sup>, Haotong Qin<sup>2,4</sup>,  
Jinjin Gu<sup>5,6</sup>, Xin Yuan<sup>7</sup>, Linghe Kong<sup>1\*</sup>, Xiaokang Yang<sup>1</sup>

<sup>1</sup>Shanghai Jiao Tong University, <sup>2</sup>ETH Zürich, <sup>3</sup>Tsinghua University, <sup>4</sup>Beihang University,  
<sup>5</sup>Shanghai AI Laboratory, <sup>6</sup>The University of Sydney, <sup>7</sup>Westlake University

## Abstract

3D whole-body human mesh recovery aims to reconstruct the 3D human body, face, and hands from a single image. Although powerful deep learning models have achieved accurate estimation in this task, they require enormous memory and computational resources. Consequently, these methods can hardly be deployed on resource-limited edge devices. In this work, we propose a Binarized Dual Residual Network (BiDRN), a novel quantization method to estimate the 3D human body, face, and hands parameters efficiently. Specifically, we design a basic unit Binarized Dual Residual Block (BiDRB) composed of Local Convolution Residual (LCR) and Block Residual (BR), which can preserve full-precision information as much as possible. For LCR, we generalize it to four kinds of convolutional modules so that full-precision information can be propagated even between mismatched dimensions. We also binarize the face and hands box-prediction network as Binarized BoxNet, which can further reduce the model redundancy. Comprehensive quantitative and qualitative experiments demonstrate the effectiveness of BiDRN, which has a significant improvement over state-of-the-art binarization algorithms. Moreover, our proposed BiDRN achieves comparable performance with full-precision method Hand4Whole while using just 22.1% parameters and 14.8% operations. The code and models will be available at <https://github.com/ZHITENGLI/BiDRN>.

## 1. Introduction

3D whole-body human mesh recovery is a fundamental task in computer vision and aims to reconstruct the 3D whole-body human mesh of a person instance from a single image or video. By recovering the 3D whole-body human mesh, we are able to understand human behaviors and feelings through their poses and expressions. Therefore, 3D whole-body human mesh recovery has been widely applied for action recognition, virtual try-on, motion retargeting, and more. In recent years, powerful deep learning models [4, 8, 23, 29, 37] have been proposed with remark-





			
Image	Hand4Whole [29]	BNN [15]	BiDRN (Ours)
Params / OPs	77.84 / 16.85	21.61 / 2.63	17.22 / 2.50

Figure 1. Visual comparison between full-precision Hand4Whole, BNN, and our BiDRN. The second line is Params (M) / OPs (G).

able accuracy. However, real-world applications like Augmented Reality (AR) require real-time responses, which necessitate the development of models that are not only accurate but also efficient with less memory and computation.

Existing 3D whole-body human mesh recovery methods can be divided into two categories, *i.e.*, optimization-based methods and regression-based methods. The latter is more efficient and is gaining more attention with the rise of SMPL [26] and SMPL-X [33] parametric models. Most regression-based models [4, 8, 29, 37, 49] contain separate body, hands, and face networks. Hands and face regions are cropped from the original image with predicted boxes. Then, they are resized into higher resolution and input to the hands and face encoders respectively to achieve better estimation. The encoder of each network extracts image features, whose quality is required, and feeds them into the decoder for regressing the corresponding body, hands, and face parameters. Finally, these parameters are fed into an SMPL-X layer [33] to obtain a 3D whole-body human mesh. Although superior performance is achieved, these methods usually have a large model size, which requires extensive computing and memory resources, especially high-end graphics processing units (GPUs). In addition, methods like Hand4Whole [29] also adopt a multi-stage pipeline with additional hand-only and face-only datasets [28, 50], which results in a more complicated system. The demand for running 3D whole-body human mesh recovery on mobile devices (with limited resources) increases rapidly. It is urgent to develop a simple yet efficient algorithm for 3D whole-body human mesh recovery while preserving the estimation accuracy as much as possible.

\*Corresponding authors: Yulun Zhang, Linghe Kong

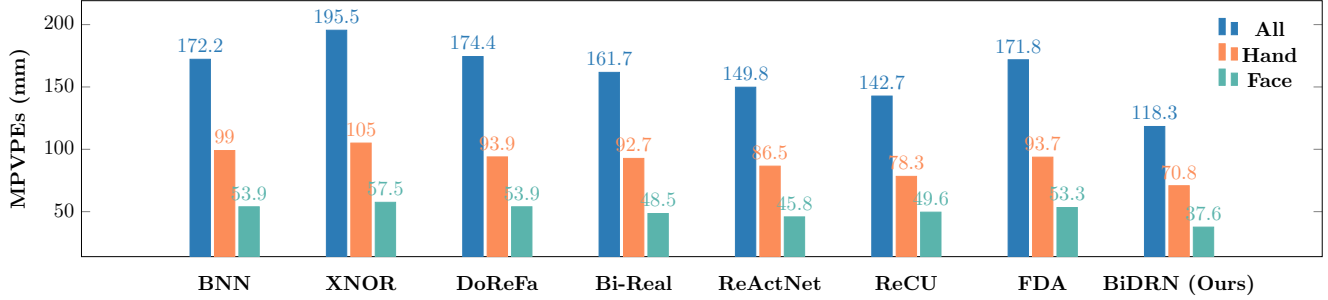


Figure 2. Comparison between recent BNNs and our BiDRN on EHF dataset. The *MPVPEs* (the lower, the better) of All, Hand, and Face are represented by blue, orange, and green colors, respectively. BiDRN significantly reduces the *All MPVPEs* of BNN [15], XNOR [36], DoReFa [48], Bi-Real [24], ReActNet [25], ReCU [44] and FDA [42] by 53.9, 77.2, 56.1, 43.4, 31.5, 24.4, and 53.5 respectively.

As the size of deep learning models increases rapidly, model compression becomes particularly important when deployed to edge devices. The study of model compression can be divided into five categories, including quantization [15, 24, 34, 35, 39, 48], knowledge distillation [3, 13, 45], pruning [9, 10, 12], lightweight network design [14, 27, 47], and low-rank approximation [5, 21, 22]. Among these five classes, the binarized neural network (BNN) is the most aggressive quantization technology that can compress memory and computational costs extremely. By quantizing the full-precision (*i.e.*, 32 bits) weights and activations into only 1 bit, BNN can achieve up to  $32\times$  memory saving and  $58\times$  speedup on center processing units (CPUs) for convolution layer [36]. In addition, bitwise operations like XNOR and bit-count can be implemented in embedded devices in an efficient manner [6, 46].

However, the direct application of network binarization for 3D whole-body human mesh recovery may encounter three challenges: (1) The quality of extracted features from the encoder is significant for parameter regression. Directly binarizing the encoder may cause severe full-precision information loss. (2) The dimension mismatch problem, when reshaping features, prevents bypassing full-precision information in BNN, which should be tackled for general situations. (3) To obtain accurate enough body, hands, and face parameters with as little memory and computation cost as possible, which parts should or should not be binarized requires careful consideration.

To address the above challenges, we propose **Binarized Dual Residual Network (BiDRN)**, a novel BNN-based methods for 3D whole-body human mesh recovery. **First**, we propose a Binarized Dual Residual Block (BiDRB), which serves as a basic unit of the network. Specifically, BiDRB can bypass full-precision activations, which is significant for body, hands, and face parameter regression, by adopting a Local Convolution Residual (LCR) with almost the same memory and computation cost. Besides, we redesign four kinds of convolutional modules and generalize them to more complicated situations, so that they can apply the LCR even for dimension mismatch situations. What's

more, BiDRB utilizes a full-precision Block Residual (BR) to further enhance the full-precision information with tolerable cost but significant improvements. **Second**, we binarized some specific layers in the hands and face box-prediction net, which can maintain the performance while reducing memory and computation costs enormously. We derive our BiDRN based on the above techniques, which has significant improvements over SOTA BNNs, with more than 31.5 *All MPVPEs* reduction, as shown in Figure 2.

Our contributions can be summarized as follows.

- We propose BiDRN, a novel BNN-based method for 3D whole-body human mesh recovery. To the best of our knowledge, this is the first work to study the binarization of whole-body human mesh recovery problem.
- We propose a new binarized unit BiDRB composed of Local Convolution Residual (LCR) and Block Residual (BR), which can maintain the full-precision information as much as possible and narrow the *All MPVPEs* gap with full-precision method from **85.9** to **32.0**.
- Our BiDRN significantly outperforms SOTA BNNs, and even achieves comparable performance with the full-precision Hand4Whole method while requiring less than a quarter of the parameters and calculations.

## 2. Related Work

### 2.1. Whole-body Human Mesh Recovery

Optimization-based methods [19, 33, 40, 41] first estimate 2D person keypoints, and then reconstruct 3D human bodies with additional constraints. Yet, these methods often involve complex optimization objectives and thus are computationally intensive. With the release of statistical human models, like SMPL [26] and SMPL-X [33], regression-based methods emerge to recover the 3D human mesh in an end-to-end manner. For example, ExPose [4] utilizes body-driven attention to extract crops of face and hand regions and part-specific knowledge from existing face- and hand-only datasets. FrankMocap [37] first runs 3D pose regression methods for body, face, and hands independently, followed by composing the regression outputs via an integration module. PIXIE [8] proposes a novel moderator to

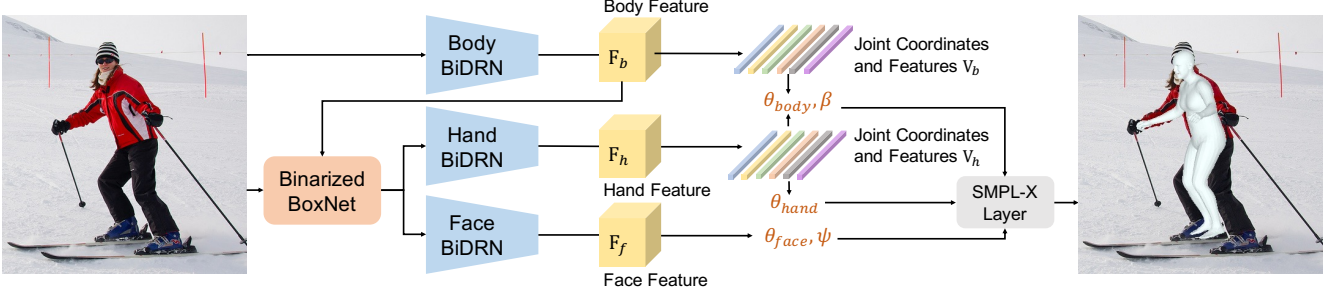


Figure 3. The overview pipeline of our binarized 3D whole-body human mesh recovery method. The body, hand, and face BiDRN serve as encoders to extract corresponding features. Binarized BoxNet predicts the face and hands regions based on body features.

fuse body part features adaptively with realistic facial details. Hand4Whole [29] produces more accurate 3D wrist rotation and smooth connection between 3D whole-body and hands by combining both body and hand MCP joint features. Although these powerful methods achieve precise results of 3D human mesh, they require powerful hardware with enormous memory and computation resources. Moreover, they utilize multi-stage pipelines for body, hands, and face estimation, which further increases the training difficulty and resource consumption. 3D whole-body human mesh recovery models that can store and run in resource-limit devices are being under-explored. This work tries to move forward in this direction.

## 2.2. Binarized Neural Network

Binarized neural networks (BNNs) [15] represent the activations and weights with only 1-bit, which is an extreme compression of computation and memory. It is first introduced in the image classification task, and several subsequent works [24, 25, 35] further push the performance on its basis. Thanks to BNN’s extreme compression of the model and relatively acceptable performance, it has been applied in other vision tasks as well. For example, Jiang *et al.* [17] utilized a BNN without batch normalization for image super-resolution. Cai *et al.* [2] designed a binarized convolution unit BiSR-Conv that can adapt the density and distribution of hyperspectral image (HSI) representations for HSI restoration. However, the potential of BNN in whole-body human mesh recovery remains unexplored.

## 3. Method

Although the present SOTA method OSX [23] offers impressive results, it is built on a vision transformer [7, 43] encoder and attention-based decoders that are difficult to be binarized. Thus, we propose our binarization model based on the previous state-of-the-art method Hand4Whole [29]. In Hand4Whole, ResNet [11] backbone is used to extract high-quality features of body, face, and hands, which is the main source of memory and computational costs. In addition, it adopts the extracted body feature to predict the bounding box of face and hands by a BoxNet, which may be

complex and can be compressed as well. Based on these observations, we propose a Binarized Dual Residual Network (BiDRN) (see Figure 3) to replace the ResNet backbone and a Binarized BoxNet. They can reduce memory and computational costs enormously while preserving accuracy.

### 3.1. Binarized Dual Residual Block

The details of BiDRB are illustrated in Figure 4. The full-precision activation input  $a_f \in \mathbb{R}^{C \times H \times W}$  is binarized into 1-bit activation by a Sign function as

$$a_b = \text{Sign}(a_f) = \begin{cases} +1, & a_f \geq 0 \\ -1, & a_f < 0 \end{cases}, \quad (1)$$

where  $a_b \in \mathbb{R}^{C \times H \times W}$  denotes the binarized activation. Quantization by Sign function can reduce the parameters extremely. However, Sign function is non-differentiable and we have to approximate it during backpropagation.

Here, we adopt a piecewise quadratic function to approximate the gradient computation of Sign function as

$$F(a_f) = \begin{cases} +1, & a_f \geq 1 \\ -a_f^2 + 2a_f, & 0 \leq a_f < 1 \\ a_f^2 + 2a_f, & -1 \leq a_f < 0 \\ -1, & a_f < -1 \end{cases}. \quad (2)$$

We notice that the gradients of activations outside range  $[-1, +1]$  vanishes, and they will not be updated during backpropagation. Another problem is that the ReLU pre-activation used by default in previous work will generate all-one activations after the Sign function. This may lead to the failure of binarization. To solve these two problems, we adopt a Hardtanh pre-activation function that can compress the full-precision activation into the range  $[-1, +1]$  as

$$a_f = \text{Hardtanh}(x_f) = \begin{cases} +1, & x_r \geq 1 \\ x_r, & -1 \leq x_r < 1 \\ -1, & x_r < -1 \end{cases}, \quad (3)$$

where  $\mathbf{X}_f \in \mathbb{R}^{C \times H \times W}$  is the output feature from previous layer. Compared with methods that use a learnable threshold before Sign function [25] or a redistribution trick [2], Hardtanh in this case can achieve better performance with-

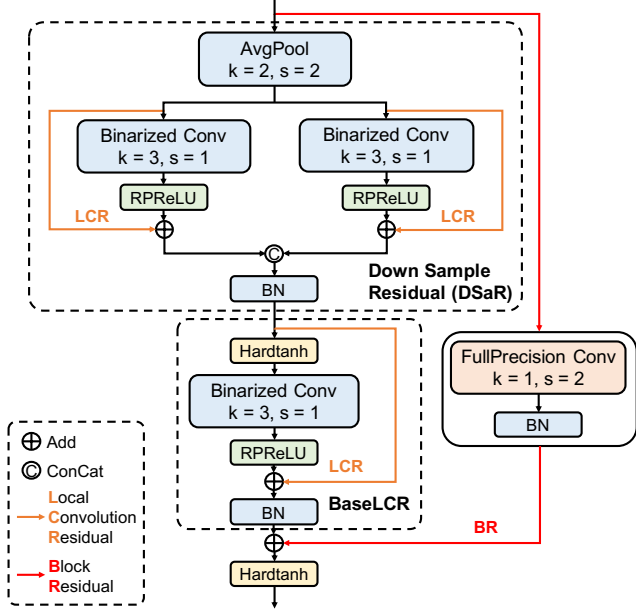


Figure 4. A kind of Binarized Dual Residual Block (BiDRB). The orange arrow denotes Local Convolution Residual (LCR), while the red arrow denotes Block Residual (BR).

out additional parameter burden.

Weights  $\mathbf{W}_f \in \mathbb{R}^{C_{in} \times C_{out} \times K \times K}$  in binarized convolution layer is also quantized into 1-bit weights  $\mathbf{W}_b$  as

$$w_b^i = \alpha^i \cdot \text{Sign}(w_f^i), \quad (4)$$

where index  $i$  represents the  $i$ -th output channel, and  $\alpha$  is a scaling factor defined as  $\alpha^i = \frac{\|w_f^i\|_1}{C_{in} \times K \times K}$ . Multiplying the channel-wise scaling factor can better maintain the original distribution on each channel.

After binarizing both activations and weights, the computation of binarized convolution can be formulated as [36]

$$\mathbf{o} = \alpha \cdot \text{bitcount}(\text{Sign}(\mathbf{a}_f) \odot \text{Sign}(\mathbf{W}_f)), \quad (5)$$

where  $\odot$  denotes the XNOR-bitcount bitwise operation and  $\mathbf{o}$  denotes the output of binarized convolution.

XNOR and bitcount are both logical operations that can obviously reduce the computation overhead of full-precision matrix multiplication. However, the loss of full-precision information in quantization is non-neglectable. Compared with the binarized information, full-precision information usually represents image details, which may not be dominant in image classification task, but is significant in 3D body mesh recovery. Since regression-based methods only optimize a few body, hands, and face parameters, small perturbations on the feature may be transmitted to the parameters and have a great impact on the final 3D mesh.

To preserve the full-precision information as much as possible, we design two kinds of residual connections, *i.e.*, Local Convolution Residual (LCR) and Block Residual (BR). We then give more details about them respectively.

**Local Convolution Residual.** This residual connection is applied to each binarized convolution layer to bypass full-precision activation. Since the value range of binarized convolution output  $\mathbf{o}$  is much smaller than the full-precision activation  $\mathbf{a}_f$ . We first apply the channel-wise RPRReLU [25] activation function to enlarge its value diversity and redistribute the representation as

$$\text{RPRReLU}(o^i) = \begin{cases} o^i - \gamma^i + \zeta^i, & o^i > \gamma^i \\ \beta^i(o^i - \gamma^i) + \zeta^i, & o^i \leq \gamma^i \end{cases}, \quad (6)$$

where  $o^i$  is the binarized convolution output of the  $i$ -th channel,  $\gamma^i, \zeta^i, \beta^i \in \mathbb{R}$  are learnable parameters. After that, the full-precision activation  $\mathbf{a}_f$  is added as

$$\mathbf{o}' = \text{BatchNorm}(\text{RPRReLU}(\mathbf{o}) + \mathbf{a}_f), \quad (7)$$

where  $\mathbf{o}'$  is the output feature. Note that the parameters introduced by RPRReLU are relatively small compared to the convolution kernels and thus can be ignored.

This local convolution residual can bypass full-precision information during the whole network if the dimension remains unchanged. Unfortunately, to extract compact image features, there exists Down Scale, Down Sample, Fusion Up, and Fusion Down operations in the encoder. The dimension mismatch problem in these modules prevents bypassing the full-precision information and thus leads to a performance drop. To tackle this problem, we redesign these modules so that they can be combined with our Local Convolution Residual, as illustrated in Figure 5.

Specifically, Down Scale module shrinks the spatial dimension. To match the output dimension, the full-precision activation is first fed into an average pooling function and then added to the output of Down Scale convolution as

$$\mathbf{o}' = \text{BatchNorm}(\text{RPRReLU}(\mathbf{o}) + \text{AvgPool}(\mathbf{a}_f)), \quad (8)$$

where  $\mathbf{o}' \in \mathbb{R}^{C \times \frac{H}{2} \times \frac{W}{2}}$ ,  $\mathbf{o}, \mathbf{a}_f \in \mathbb{R}^{C \times H \times W}$ . Note that the average pooling function does not introduce any additional parameter and its computational cost can be ignored compared to the large encoder.

For Fusion Up which increases the channel dimension, we replace the convolution layer with two distinct layers. We make each layer's output channel equal to the input channel so that they can reuse the normal LCR. Finally, they are concatenated in channel dimension as

$$\mathbf{o}' = \text{BatchNorm}(\text{Concat}(\mathbf{o}'_1, \mathbf{o}'_2)), \quad (9)$$

where  $\mathbf{o}' \in \mathbb{R}^{2C \times H \times W}$ ,  $\mathbf{o}'_1, \mathbf{o}'_2 \in \mathbb{R}^{C \times H \times W}$ .

Fusion Down is the inverse of Fusion Up, thus we first split the input in channel dimension and then feed them into two distinct binarized convolution layers with Local Convolution Residual. Finally, they are summed up as

$$\mathbf{o}' = \text{BatchNorm}(\mathbf{o}'_1 + \mathbf{o}'_2), \quad (10)$$

where  $\mathbf{o}' \in \mathbb{R}^{\frac{C}{2} \times H \times W}$ ,  $\mathbf{o}'_1, \mathbf{o}'_2 \in \mathbb{R}^{\frac{C}{2} \times H \times W}$ .



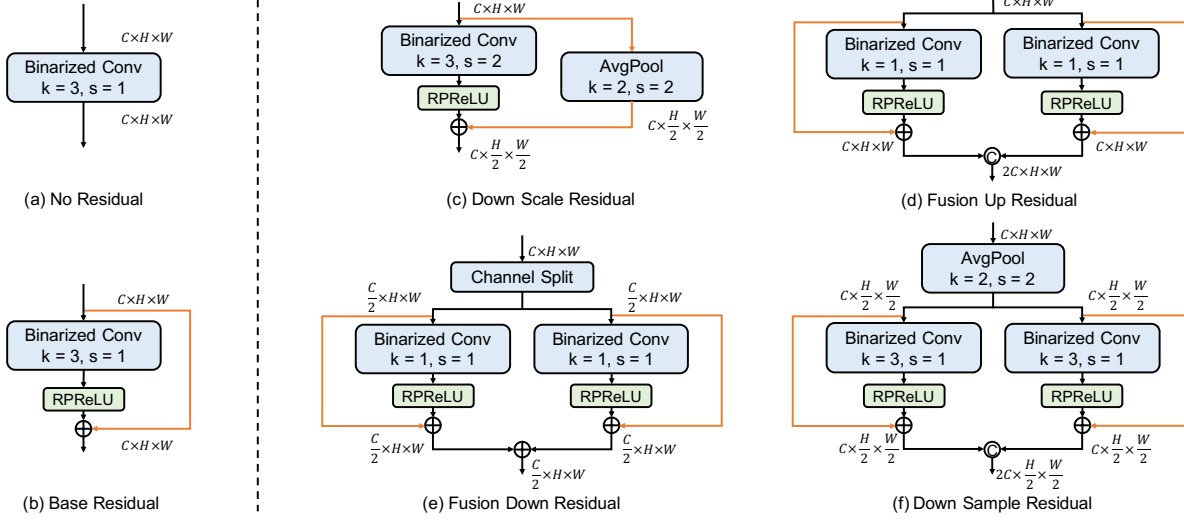


Figure 5. Illustration of our base Local Convolution (Base) Residual and four redesign modules, including (c) Down Scale Residual (DSrR), (d) Fusion Up Residual (FUR), (e) Fusion Down Residual (FDR), and (f) Down Sample Residual (DSaR). The orange arrow denotes the full-precision information flow. For simplicity, batch normalization and Hardtanh pre-activation are omitted.

Down Sample is the mix of Down Scale and Fusion Up, thus we first apply the average pooling and then use channel concatenation. Note that we just describe the condition of double or half the size for simplicity, while it is generalized to more complex conditions with four times channels in BiDRN. By redesigning these four modules, we are able to bypass the full-precision activations with almost the same parameter and computational cost.

**Block Residual.** Full-precision information may be obscured or diluted by binarized convolution layers, especially after a very deep network. So, we further propose a Block Residual to bypass full-precision information in each block.

Note that the number of blocks is much smaller than that of convolution layers, we utilize a full-precision Conv1×1 to extract more accurate features with acceptable parameter burden. As shown in Figure 4, the overall BiDRB composed of LCR and BR can be formulated as

$$o'' = \text{BaseLCR}(\text{DSaR}(a_f)) + \text{BR}(a_f), \quad (11)$$

where BaseLCR, DSaR, and BR denote base Local Convolution Residual, Down Sample Residual, and Block Residual respectively. Note that Equation (11) is only one kind of BiDRB, other kinds of BiDRB may combine with Fusion up, Fusion Down, and Down Scale Residuals. It should be noted here. A binarized version of Block Residual can be used for tasks that do not require high-quality features but require efficiency with extreme compression.

Combining both Local Convolution Residual and Block Residual, Binarized Dual Residual Block can preserve full-precision information as much as possible with almost the same parameters and computation. The body, hand, and face encoders that build on BiDRN can extract better image features than simple binarization methods.

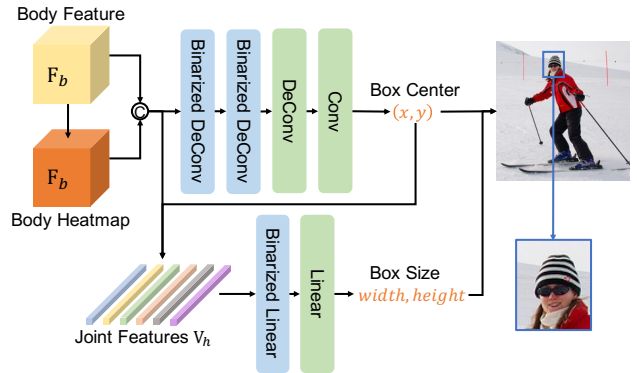


Figure 6. Binarized face BoxNet extracts the face region from the high-resolution human image. Hands regions are extracted by binarized hands BoxNet with the same architecture.

### 3.2. Binarized BoxNet

The bounding boxes of hands and face are predicted by the BoxNet. It first predicts 3D heatmaps of human joints  $\mathbf{H}$  from the output of encoder  $\mathbf{F}$ , then applies several Deconv and Conv layers on the concatenation of  $\mathbf{H}$  and  $\mathbf{F}$ . After that, soft-argmax [38] is applied to obtain the box center, and full-connected layers are applied to obtain the box size. We observe that the parameters and computation of these layers are very large compared with other components in the decoder, especially the DeConv layers, which seem a bit redundant for just calculating several box parameters.

Therefore, as shown in Figure 6, we binarize both the Deconv layers and Linear layers except the final one, so that we can obtain good output accuracy. Our experiments (see Table 3) further show that the binarization here even leads to performance gain and meanwhile reduces memory and computational costs significantly.

Method	Bit	Params (M)	OPs (G)	EHF								AGORA					
				MPVPE ↓			PA-MPVPE ↓			PA-MPJPE ↓		MPVPE ↓			PA-MPVPE ↓		
				All	Hand	Face	All	Hand	Face	Body	Hand	All	Hand	Face	All	Hand	Face
ExPose [4]	32	-	-	77.1	51.6	35.0	54.5	12.8	5.8	-	-	219.8	115.4	103.5	88.0	12.1	4.8
FrankMocap [37]	32	-	-	107.6	42.8	-	57.5	12.6	-	-	-	218.0	95.2	105.4	90.6	11.2	4.9
PIXIE [8]	32	-	-	89.2	42.8	32.7	55.0	11.1	4.6	-	-	203.0	89.9	95.4	82.7	12.8	5.4
Hand4Whole [29]†	32	77.84	16.85	86.3	47.2	26.1	57.5	13.2	5.8	70.9	13.3	194.8	78.6	88.3	79.0	9.8	4.8
BNN [15]	1	21.61	2.63	172.2	99.0	53.9	115.6	18.4	6.2	129.4	19.0	267.6	114.0	141.3	94.9	10.4	5.0
XNOR [36]	1	21.61	2.63	195.5	105.0	57.5	119.9	18.5	6.2	134.5	19.1	271.1	127.9	156.9	94.1	10.5	5.1
DoReFa [48]	1	21.61	2.63	174.4	93.9	53.9	109.3	18.4	6.0	121.3	19.0	257.6	115.3	139.4	93.5	10.4	5.0
Bi-Real [24]	1	21.61	2.63	161.7	92.7	48.5	108.7	18.5	5.9	121.2	19.1	242.0	104.3	121.8	92.6	10.4	5.0
ReActNet [25]	1	21.66	2.63	149.8	86.5	45.8	98.8	18.5	6.1	111.6	19.1	237.6	102.9	120.2	91.4	10.4	4.9
ReCU [44]	1	21.71	2.65	142.7	78.3	49.6	85.4	18.2	6.0	97.1	18.8	225.1	96.2	108.3	89.7	10.3	4.9
FDA [42]	1	32.06	2.81	171.8	93.7	53.3	108.5	18.4	6.1	120.5	19.0	256.4	114.6	138.6	93.0	10.4	5.0
BiDRN (Ours)	1	17.22	2.50	118.3	70.8	37.6	76.9	17.4	6.0	88.2	17.9	215.0	92.1	102.3	87.7	10.3	4.9

Table 1. 3D whole-body reconstruction error comparisons on EHF [33] and AGORA [32] whole-body evaluation benchmarks. † It does not use pre-trained weights, as well as additional hand-only and face-only datasets for fair comparison.

## 4. Experiment

### 4.1. Experimental Settings

**Datasets.** For training, we adopt Human3.6M [16], whole-body MSCOCO [18] and MPII [1]. Following [29], the 3D pseudo-GTs for training are obtained by NeuralAnnot [30]. To make the binarized model simple and easy to train, unlike [29], we do not use additional hand-only and face-only datasets, as well as additional stages to finetune the model. Finally, we use EHF [33] and AGORA [32] for evaluation.

**Evaluation Metrics.** We adopt Mean per joint position error (MPJPE), mean per-vertex position error (MPVPE), and their aligned version PA MPJPE, PA MPVPE to evaluate the performance of 3D whole-body human mesh recovery. Following [2, 15, 35, 39], we calculate the parameters of BNNs by  $\text{Params} = \text{Params}_b + \text{Params}_f$ , where  $\text{Params}_b = \text{Params}_f / 32$  represents that the binarized parameters is 1/32 of its full-precision counterpart. Similarly, the computational complexity of BNNs is measured by operation per second (OPs), which is calculated by  $\text{OPs} = \text{OPs}_b + \text{OPs}_f$ , where  $\text{OPs}_b = \text{OPs}_f / 64$ , and  $\text{OPs}_f = \text{FLOPs}$ .

**Implementation Details.** Our BiDRN is implemented in PyTorch [31]. To be consistent with the efficient concept of binarized networks, we do not pre-train it on any dataset, nor finetune by additional hand-only and face-only datasets. We use Adam [20] optimizer with batch size 24 and initial learning rate of  $1 \times 10^{-4}$  to train BiDRN for 14 epochs on a single A100 GPU. We use scaling, rotation, random horizontal flip, and color jittering for data augmentations.

### 4.2. Quantitative Results

We compare our BiDRN with 7 SOTA BNN-based methods, including BNN [15], XNOR [36], DoReFa [48], Bi-Real [24], ReActNet [25], ReCU [44], and FDA [42]. Besides, we also compare BiDRN with 4 SOTA 32-bit full-precision methods, including ExPose [4], FrankMocap [37], PIXIE [8], and Hand4Whole [29].

Table 1 presents the performance comparisons on both EHF and AGORA datasets. It can be observed that although existing SOTA BNN-based methods can compress the model to only 27.8% (21.61/77.84) of the original Params and 15.6% (2.63/16.85) of the original OPs, directly applying them to the 3D mesh recovery task achieves poor performance. While our BiDRN surpasses these methods by large margins with even fewer Params and OPs. Specifically, the *All MPVPEs* of BiDRN show 31.3%, 39.5%, 32.2%, 26.8%, 21.0%, 17.1%, and 31.1% improvements than BNN, XNOR, DoReFa, Bi-Real, ReActNet, ReCU, and FDA on EHF dataset respectively. For the AGORA dataset, BiDRN also outperforms 7 SOTA BNN-based methods. Compared to the most basic BNN algorithm, the *MPVPEs* of our BiDRN show 19.7%, 19.2%, and 27.6% improvements on body, hands, and face respectively.

When compared to the 32-bit full-precision methods, the proposed BiDRN also achieves comparable performance with extremely lower memory and computational cost. For the EHF dataset, BiDRN narrows the *All MPVPEs* gap between full-precision Hand4Whole and binarization methods from 85.9 to 32.0. For the AGORA dataset, surprisingly, our BiDRN even surpasses ExPose and FrankMocap. As AGORA is a more complex and natural dataset [29, 32], it can better demonstrate the effectiveness of our BiDRN.

### 4.3. Qualitative Results

We follow previous work [23, 29] to show the qualitative results on MSCOCO dataset, as depicted in Figure 7. It can be observed that the 3D human meshes recovered by previous BNN methods cannot even match the 2D images, resulting in completely incorrect results. While our BiDRN can match all 2D images well, even with complex backgrounds such as the fourth and final rows. In addition, previous BNN methods may generate wrong rotations, e.g. the third and fifth rows. While our BiDRN keeps the original rotations with more accurate facial expressions and hand poses. Fi-





Figure 7. Qualitative results comparison between seven SOTA BNN-based methods and our proposed BiDRN on MSCOCO [18] dataset. Bypassing the full-precision information is necessary for accurate whole-body human mesh recovery.

nally, BiDRN is more stable than other BNNs, and achieves accurate and consistent estimations in all images.

#### 4.4. Ablation Study

**Break-down Ablation.** We first build up a baseline with base Local Convolution Residual. Then we successively use our Down Scale Residual (DScR), Fusion Up Residual (FUR), Fusion Down Residual (FDR), and Down Sample Residual (DSaR) to enhance the performance. Notice that the *All MPVPEs* of our BaseLCR (139.3) already outperforms the basic BNN method (172.2) by a large margin. As shown in Table 2a, when we successively use DScR, FUR, FDR, and DSaR, the *All MPVPEs* is reduced by 11.5, 1.8, 1.3, and 6.4. As shown in Figure 8, the BaseLCR can al-



Figure 8. Visual comparison of break-down ablation study.

ready match the 2D image roughly, and successively adding these four modules can fine-tune the body rotation, hand position, and leg angle step by step. Adding all these modules reduces the *All MPVPEs* by 21.0 in total with just a few additional Params and OPs, which demonstrates the effectiveness of our LCR and its four derived modules.

**Pre-activation.** We compare the Hardtanh used in our

Method	BaseLCR	+ DScR	+ FUR	+ FDR	+ DSaR
All MPVPEs	139.3	127.8	126.0	124.7	118.3
Params (M)	17.05	17.05	17.14	17.21	17.22
OPs (G)	2.48	2.48	2.49	2.50	2.50

(a) Break-down ablation of Local Convolution Residual (LCR)

Method	Params (M)	OPs (G)	All	Hand	Face
w/o BR	11.51	1.25	139.6	85.4	39.1
Binarized BR	11.68	1.28	120.0	73.3	37.9
Full-precision BR	17.22	2.50	118.3	70.8	37.6

(c) Ablation study of Block Residual (BR)

Method	Additional Params	All	Hand	Face
Hardtanh( $x_f$ )	No	118.3	70.8	37.6
ReLU( $x_f$ )	No	126.8	71.5	38.9
PReLU( $x_f$ )	Yes	125.9	70.6	37.3

(b) Study of pre-activation function

Binarized Network	Params (M)	OPs (G)	All	Hand	Face
Body Encoder	47.78	7.45	119.8	65.9	36.7
Hand Encoder	47.78	7.45	86.0	49.0	27.9
Face Encoder	57.08	9.94	86.8	55.3	25.9

(d) Ablation study of binarizing different parts of BiDRN

Table 2. Ablations on EHF dataset, all experiments are evaluated in *MPVPEs*. In table (a), DScR, FUR, FDR, and DSaR denote the Down Scale Residual, Fusion Up Residual, Fusion Down Residual, and Down Sample Residual of Figure 5. In table (d), the *MPVPEs* of binarizing all networks are 122.6, 68.6, 39.6 for All, Hand, and Face respectively.

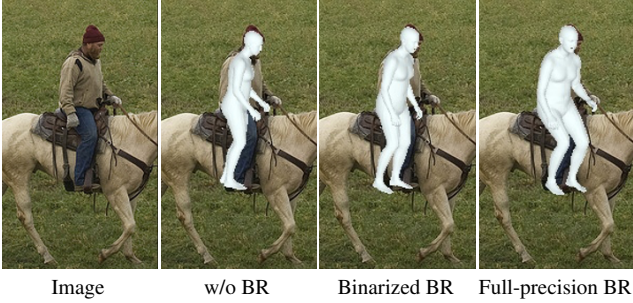


Figure 9. Visual comparison of Block Residual ablation study.

BiDRN with previous default pre-activation functions ReLU and PReLU. As shown in Table 2b, when replacing ReLU or PReLU with Hardtanh, the *All MPVPEs* can be reduced by 8.5 and 7.6 respectively without additional parameters. This suggests the superiority of Hardtanh pre-activation in binarization methods.

**Block Residual.** To study the effect of Block Residual, we remove it from BiDRN, and also compare it with its binarization counterpart. It can be observed from Table 2c that without Block Residual, our method can still achieve 139.6 *All MPVPEs*, which surpasses basic BNN (172.2) with just half of the Params and OPs. When adding binarized BR, the *All MPVPEs* can be reduced by 19.6, which is a significant improvement with just a few additional Params and OPs. By replacing the binarized BR with full-precision BR, the *All MPVPEs* can be further reduced by 1.7. Although the improvement of full-precision is not particularly large in quantitative results, the qualitative results in Figure 9 show that full-precision is still very important for accurate 3D human mesh recovery. It can be observed that only Full-precision BR recovers the accurate hand position and rotation, while Binarized BR only recovers the body well.

**Binarizing Different Networks.** Since body, hand, and face use separate encoder networks, we binarize one of them while keeping the other two as full-precision to study the binarization benefit. The experimental results are listed in Table 2d, we can observe that (1) Binarizing the encoder leads to a corresponding performance drop. However, the *MPVPE* of face is improved when binarizing Face Encoder,

Method	Params (M)	OPs (G)	All	Hand	Face
Full-precision BoxNet	21.81	1.87	130.7	78.4	40.5
Binarized BoxNet	11.68	1.28	125.5	75.1	39.0

Table 3. Abalation study of BoxNet on EHF. Both binarized and full-precision BoxNets are trained with Binarized Block Residual.

suggesting that the full-precision face encoder has many parameter and operation redundancies, and our binarization method can already retain full-precision information well. (2) The binarization of Body Encoder also leads to a performance drop of hand and face. On the contrary, binarization of the Hand or Face Encoder has little impact on other parts. This suggests that the body encoder is the key point of 3D human mesh recovery since the face and hands boxes are predicted by body feature. Therefore, the full-precision information on body feature is more important.

**BoxNet.** To further verify the effectiveness of our Binarized BoxNet, we compare it with the full-precision BoxNet. As shown in Table 3, Binarized BoxNet achieves even better performance with much fewer parameters and operations, which suggests that the full-precision BoxNet is redundant and will lead to a performance drop.

## 5. Conclusion

In this work, we propose BiDRN, a novel BNN-based method for 3D whole-body human mesh recovery. To the best of our knowledge, this is the first work to study the binarization of 3D whole-body human mesh recovery problem. To maintain the full-precision information as much as possible, we present a new binarized unit BiDRB with Local Convolution Residual and Block Residual. Comprehensive quantitative and qualitative experiments demonstrate that our BiDRN significantly outperforms SOTA BNNs and even achieves comparable performance with full-precision 3D whole-body human mesh recovery methods.

**Limitation and future work.** Currently, our BiDRN does not improve the estimation accuracy of different parts uniformly. The enhancement of hand estimation is smaller than that of the body and face. It is worth studying how to further improve hand estimation accuracy in future work.



## References

- [1] Mykhaylo Andriluka, Leonid Pishchulin, Peter Gehler, and Bernt Schiele. 2d human pose estimation: New benchmark and state of the art analysis. In *CVPR*, 2014. 6
- [2] Yuanhao Cai, Yuxin Zheng, Jing Lin, Haoqian Wang, Xin Yuan, and Yulun Zhang. Binarized spectral compressive imaging. *NeurIPS*, 2023. 3, 6
- [3] Yuntao Chen, Naiyan Wang, and Zhaoxiang Zhang. Dark-rank: Accelerating deep metric learning via cross sample similarities transfer. In *AAAI*, 2018. 2
- [4] Vasileios Choutas, Georgios Pavlakos, Timo Bolkart, Dimitrios Tzionas, and Michael J Black. Monocular expressive body regression through body-driven attention. In *ECCV*, 2020. 1, 2, 6
- [5] Emily L Denton, Wojciech Zaremba, Joan Bruna, Yann LeCun, and Rob Fergus. Exploiting linear structure within convolutional networks for efficient evaluation. *NeurIPS*, 2014. 2
- [6] Ruizhou Ding, Ting-Wu Chin, Zeye Liu, and Diana Marculescu. Regularizing activation distribution for training binarized deep networks. In *CVPR*, 2019. 2
- [7] Alexey Dosovitskiy, Lucas Beyer, Alexander Kolesnikov, Dirk Weissenborn, Xiaohua Zhai, Thomas Unterthiner, Mostafa Dehghani, Matthias Minderer, Georg Heigold, Sylvain Gelly, et al. An image is worth 16x16 words: Transformers for image recognition at scale. *ICLR*, 2021. 3
- [8] Yao Feng, Vasileios Choutas, Timo Bolkart, Dimitrios Tzionas, and Michael J Black. Collaborative regression of expressive bodies using moderation. In *3DV*, 2021. 1, 2, 6
- [9] Song Han, Jeff Pool, John Tran, and William Dally. Learning both weights and connections for efficient neural network. *NeurIPS*, 2015. 2
- [10] Song Han, Huizi Mao, and William J Dally. Deep compression: Compressing deep neural networks with pruning, trained quantization and huffman coding. *ICLR*, 2016. 2
- [11] Kaiming He, Xiangyu Zhang, Shaoqing Ren, and Jian Sun. Deep residual learning for image recognition. In *CVPR*, 2016. 3
- [12] Yihui He, Xiangyu Zhang, and Jian Sun. Channel pruning for accelerating very deep neural networks. In *ICCV*, 2017. 2
- [13] Geoffrey Hinton, Oriol Vinyals, and Jeff Dean. Distilling the knowledge in a neural network. *NeurIPS*, 2015. 2
- [14] Andrew G Howard, Menglong Zhu, Bo Chen, Dmitry Kalenichenko, Weijun Wang, Tobias Weyand, Marco Andreetto, and Hartwig Adam. Mobilenets: Efficient convolutional neural networks for mobile vision applications. *arXiv preprint arXiv:1704.04861*, 2017. 2
- [15] Itay Hubara, Matthieu Courbariaux, Daniel Soudry, Ran El-Yaniv, and Yoshua Bengio. Binarized neural networks. *NeurIPS*, 2016. 1, 2, 3, 6, 7
- [16] Catalin Ionescu, Dragos Papava, Vlad Olaru, and Cristian Sminchisescu. Human3.6m: Large scale datasets and predictive methods for 3d human sensing in natural environments. *TPAMI*, 2014. 6
- [17] Xinrui Jiang, Nannan Wang, Jingwei Xin, Keyu Li, Xi Yang, and Xinbo Gao. Training binary neural network without batch normalization for image super-resolution. In *AAAI*, 2021. 3
- [18] Sheng Jin, Lumin Xu, Jin Xu, Can Wang, Wentao Liu, Chen Qian, Wanli Ouyang, and Ping Luo. Whole-body human pose estimation in the wild. In *ECCV*, 2020. 6, 7
- [19] Hanbyul Joo, Tomas Simon, and Yaser Sheikh. Total capture: A 3d deformation model for tracking faces, hands, and bodies. In *CVPR*, 2018. 2
- [20] Diederik P Kingma and Jimmy Ba. Adam: A method for stochastic optimization. *ICLR*, 2015. 6
- [21] Vadim Lebedev and Victor Lempitsky. Fast convnets using group-wise brain damage. In *CVPR*, 2016. 2
- [22] Vadim Lebedev, Yaroslav Ganin, Maksim Rakhuba, Ivan Osledeets, and Victor Lempitsky. Speeding-up convolutional neural networks using fine-tuned cp-decomposition. *ICLR*, 2015. 2
- [23] Jing Lin, Ailing Zeng, Haoqian Wang, Lei Zhang, and Yu Li. One-stage 3d whole-body mesh recovery with component aware transformer. In *CVPR*, 2023. 1, 3, 6
- [24] Zechun Liu, Baoyuan Wu, Wenhan Luo, Xin Yang, Wei Liu, and Kwang-Ting Cheng. Bi-real net: Enhancing the performance of 1-bit cnns with improved representational capability and advanced training algorithm. In *ECCV*, 2018. 2, 3, 6, 7
- [25] Zechun Liu, Zhiqiang Shen, Marios Savvides, and Kwang-Ting Cheng. Reactnet: Towards precise binary neural network with generalized activation functions. In *ECCV*, 2020. 2, 3, 4, 6, 7
- [26] Matthew Loper, Naureen Mahmood, Javier Romero, Gerard Pons-Moll, and Michael J Black. Smpl: A skinned multi-person linear model. In *TOG*. 2023. 1, 2
- [27] Ningning Ma, Xiangyu Zhang, Hai-Tao Zheng, and Jian Sun. Shufflenet v2: Practical guidelines for efficient cnn architecture design. In *ECCV*, 2018. 2
- [28] Gyeongsik Moon, Shou-I Yu, He Wen, Takaaki Shiratori, and Kyoung Mu Lee. Interhand2.6m: A dataset and baseline for 3d interacting hand pose estimation from a single rgb image. In *ECCV*, 2020. 1
- [29] Gyeongsik Moon, Hongsuk Choi, and Kyoung Mu Lee. Accurate 3d hand pose estimation for whole-body 3d human mesh estimation. In *CVPR*, 2022. 1, 3, 6
- [30] Gyeongsik Moon, Hongsuk Choi, and Kyoung Mu Lee. Neuralannot: Neural annotator for 3d human mesh training sets. In *CVPR*, 2022. 6
- [31] Adam Paszke, Sam Gross, Francisco Massa, Adam Lerer, James Bradbury, Gregory Chanan, Trevor Killeen, Zeming Lin, Natalia Gimelshein, Luca Antiga, et al. Pytorch: An imperative style, high-performance deep learning library. *NeurIPS*, 2019. 6
- [32] Priyanka Patel, Chun-Hao P Huang, Joachim Tesch, David T Hoffmann, Shashank Tripathi, and Michael J Black. Agora: Avatars in geography optimized for regression analysis. In *CVPR*, 2021. 6
- [33] Georgios Pavlakos, Vasileios Choutas, Nima Ghorbani, Timo Bolkart, Ahmed AA Osman, Dimitrios Tzionas, and Michael J Black. Expressive body capture: 3d hands, face, and body from a single image. In *CVPR*, 2019. 1, 2, 6

- [34] Haotong Qin, Ruihao Gong, Xianglong Liu, Xiao Bai, Jingkuan Song, and Nicu Sebe. Binary neural networks: A survey. *Pattern Recognition*, 2020. 2
- [35] Haotong Qin, Ruihao Gong, Xianglong Liu, Mingzhu Shen, Ziran Wei, Fengwei Yu, and Jingkuan Song. Forward and backward information retention for accurate binary neural networks. In *CVPR*, 2020. 2, 3, 6
- [36] Mohammad Rastegari, Vicente Ordonez, Joseph Redmon, and Ali Farhadi. Xnor-net: Imagenet classification using binary convolutional neural networks. In *ECCV*, 2016. 2, 4, 6, 7
- [37] Yu Rong, Takaaki Shiratori, and Hanbyul Joo. Frankmocap: A monocular 3d whole-body pose estimation system via regression and integration. In *ICCV*, 2021. 1, 2, 6
- [38] Xiao Sun, Bin Xiao, Fangyin Wei, Shuang Liang, and Yichen Wei. Integral human pose regression. In *ECCV*, 2018. 5
- [39] Bin Xia, Yulun Zhang, Yitong Wang, Yapeng Tian, Wenming Yang, Radu Timofte, and Luc Van Gool. Basic binary convolution unit for binarized image restoration network. *ICLR*, 2023. 2, 6
- [40] Donglai Xiang, Hanbyul Joo, and Yaser Sheikh. Monocular total capture: Posing face, body, and hands in the wild. In *CVPR*, 2019. 2
- [41] Hongyi Xu, Eduard Gabriel Bazavan, Andrei Zanfir, William T Freeman, Rahul Sukthankar, and Cristian Sminchisescu. Ghum & ghuml: Generative 3d human shape and articulated pose models. In *CVPR*, 2020. 2
- [42] Yixing Xu, Kai Han, Chang Xu, Yehui Tang, Chunjing Xu, and Yunhe Wang. Learning frequency domain approximation for binary neural networks. *NeurIPS*, 2021. 2, 6, 7
- [43] Yufei Xu, Jing Zhang, Qiming Zhang, and Dacheng Tao. Vit-pose: Simple vision transformer baselines for human pose estimation. *NeurIPS*, 2022. 3
- [44] Zihan Xu, Mingbao Lin, Jianzhuang Liu, Jie Chen, Ling Shao, Yue Gao, Yonghong Tian, and Rongrong Ji. Recu: Reviving the dead weights in binary neural networks. In *ICCV*, 2021. 2, 6, 7
- [45] Sergey Zagoruyko and Nikos Komodakis. Paying more attention to attention: Improving the performance of convolutional neural networks via attention transfer. *ICLR*, 2017. 2
- [46] Jianhao Zhang, Yingwei Pan, Ting Yao, He Zhao, and Tao Mei. dabnn: A super fast inference framework for binary neural networks on arm devices. In *ACM MM*, 2019. 2
- [47] Xiangyu Zhang, Xinyu Zhou, Mengxiao Lin, and Jian Sun. Shufflenet: An extremely efficient convolutional neural network for mobile devices. In *CVPR*, 2018. 2
- [48] Shuchang Zhou, Yuxin Wu, Zekun Ni, Xinyu Zhou, He Wen, and Yuheng Zou. Dorefa-net: Training low bitwidth convolutional neural networks with low bitwidth gradients. *arXiv preprint arXiv:1606.06160*, 2016. 2, 6, 7
- [49] Yuxiao Zhou, Marc Habermann, Ikhsanul Habibie, Ayush Tewari, Christian Theobalt, and Feng Xu. Monocular real-time full body capture with inter-part correlations. In *CVPR*, 2021. 1
- [50] Christian Zimmermann, Duygu Ceylan, Jimei Yang, Bryan Russell, Max Argus, and Thomas Brox. Freihand: A dataset

for markerless capture of hand pose and shape from single rgb images. In *ICCV*, 2019. 1